INTERNATIONAL JOURNAL FOR NUMERICAL METHODS IN FLUIDS
Int. J. Numer. Meth. Fluids **31**: 1333–1353 (1999)

AN EXPERIMENTAL AND NUMERICAL INVESTIGATION OF CONTAINER FILLING WITH VISCOUS LIQUIDS

M.F. TOMÉ[a], S. McKEE[b,*], L. BARRATT[c], D.A. JARVIS[c] AND A.J. PATRICK[c]

[a] *Departamento de Matematica, Instituto Superior Tecnico, Lisboa, Portugal*
[b] *Department of Mathematics, University of Strathclyde, Livingstone Tower, 26 Richmond Street, Glasgow G1 1XH, UK*
[c] *Unilever Research, Colworth House, Sharnbrook, Bedfordshire, UK*

SUMMARY

This work is concerned with a study of container filling, with particular reference to the food industry. A computer code was developed and an experimental rig was built, the main purpose being to validate the software. The computational fluid dynamic (CFD) code, called GENSMAC, was specifically designed for relatively slow viscous flow and was capable of capturing multiple free surfaces. This paper focuses on the design of the experimental rig and how it functions. The visual output of the code is then compared with high-speed photographic shots of glucose syrup being jetted into a tub for a selected number of flow regimes. Copyright © 1999 John Wiley & Sons, Ltd.

KEY WORDS: Navier–Stokes; free surface flow; finite difference method; marker-and-cell method

1. INTRODUCTION

The final stage in the manufacture of many food or domestic products invariably involves filling containers. It is clearly important to fill these tubs as rapidly as possible without spillage or deterioration in the product. Filling is commonly performed by a moving dosing head extruding a jet of the product in fluid form. Problems that can arise are splashing, spluttering, sloshing and doming; jet buckling is also undesirable as it can lead to air entrainment and provoke incomplete filling. To study this problem an attack was made on two fronts: a computational fluid dynamic (CFD) code called GENSMAC was developed with the specific capability of simulating (multiple) free surfaces and an experimental rig was designed and built.

This paper discusses both, but the principal emphasis is on the equipment, which is described in detail; a full description of the code may be found elsewhere (see Tomé and McKee [1]). However, since the experimental rig was built to validate the code, which had already been written, we begin with a brief history and description of GENSMAC. The trials are restricted to Newtonian fluids. Section 2 describes the code GENSMAC and Section 3 presents results of a number of simulations performed by the GENSMAC code on container filling. Section 4 is concerned with modelling Newtonian fluids, while Section 5 gives details of the experimental set-up. Section 6 presents the procedure and the difficulties found in the

* Correspondence to: Department of Mathematics, University of Strathclyde, Livingstone Tower, 26 Richmond Street, Glasgow G1 1XH, UK.

CCC 0271–2091/99/241333–21$17.50

Received February 1998
Revised July 1998

experimental results. Finally, Section 7 presents comparisons between numerical and experimental results, and in Section 8 a general discussion of the results is given.

2. THE CFD CODE, GENSMAC

GENSMAC is an updated version of the marker-and-cell (MAC) method due originally to Harlow and Welch [2]. It is a finite difference technique based on a staggered grid and solves the full Navier–Stokes equations using the primitive variables of pressure and velocity. It is particularly adept at solving problems with free surfaces. One of the key features is the use of virtual particles, whose co-ordinates are stored and which move from one cell to the next according to the latest computed velocity components. If a cell contains a particle it is deemed to contain fluid, thus providing flow visualization of the free surface.

Over the intervening years there has been continued interest in the MAC method resulting in considerable development and refinement. A reasonably complete bibliography may be found in Tomè and McKee [1]. GENSMAC contains many novel features, such as an automatic time stepping procedure and a conjugate gradient solver for the Poisson equation. It can deal with non-rectangular domains and it is written in structured FORTRAN. It is also capable of solving non-Newtonian flows (see Tomè *et al.* [3]). Other features include sloshing (see Tomé and McKee [1]), while an extensive study of planar jet buckling may be found in Tomé and McKee [4]. Consequently, only a brief discussion of the algorithm is given here.

The basic equations of a two-dimensional time-dependent incompressible viscous flow are the Navier–Stokes equations, together with the continuity equation, which in non-dimensional form may be written as

$$\frac{\partial u}{\partial t}+\frac{\partial (u^2)}{\partial x}+\frac{\partial (uv)}{\partial y}=-\frac{\partial \phi}{\partial x}+\left(\frac{1}{Re}\right)\frac{\partial}{\partial y}\left(\frac{\partial u}{\partial y}-\frac{\partial v}{\partial x}\right)+\frac{1}{Fr^2}g_x, \tag{1}$$

$$\frac{\partial v}{\partial t}+\frac{\partial (uv)}{\partial x}+\frac{\partial (v^2)}{\partial y}=-\frac{\partial \phi}{\partial y}-\left(\frac{1}{Re}\right)\frac{\partial}{\partial x}\left(\frac{\partial u}{\partial y}-\frac{\partial v}{\partial x}\right)+\frac{1}{Fr^2}g_y, \tag{2}$$

$$\frac{\partial u}{\partial x}+\frac{\partial v}{\partial y}=0, \tag{3}$$

where $Re = UL/v$ and $Fr = U/\sqrt{Lg}$ are the associated Reynolds number and the Froude number respectively; U and L are typical velocity and length scales, v is the kinematic viscosity, g is the gravitational constant with $\mathbf{g} = (g_x, g_y)^T$ as the unit gravitational vector, and $\mathbf{u} = (u, v)^T$ are the non-dimensional components of velocity, while ϕ is the non-dimensional pressure per unit density.

To solve Equations (1)–(3) we employ a finite difference method (FDM) based on a staggered grid. Details of the methodology and the precise finite difference equations employed can be found in Tomé and McKee [1].

The basic idea of GENSMAC is as follows. Suppose that at a given time, say t_n, the velocity field $\mathbf{u}(\mathbf{x}, t_n)$ is known and boundary conditions for the velocity and pressure are given. The updated velocity field $\mathbf{u}(\mathbf{x}, t_{n+1})$, where $t_{n+1} = t_n + \delta t_n$, is calculated as follows:

(i) Let $\tilde{\phi}(\mathbf{x}, t_{n+1})$ be an arbitrary pressure field that satisfies the correct pressure condition on the free surface. This pressure field is computed from a local approximation to the stress conditions

$$\mathbf{n}\cdot\underline{\underline{\boldsymbol{\sigma}}}\cdot\mathbf{n}=0 \quad \text{and} \quad \mathbf{m}\cdot\underline{\underline{\boldsymbol{\sigma}}}\cdot\mathbf{n}=0,$$

where $\underline{\underline{\boldsymbol{\sigma}}}$ is the stress tensor; **n** and **m** are local unit normal and tangential vectors to the free surface respectively.

(ii) Calculate the intermediate velocity field, $\tilde{\mathbf{u}}(\mathbf{x}, t_{n+1})$, from a finite difference discretization of

$$\frac{\partial \tilde{u}}{\partial t} = \left[-\frac{\partial(u^2)}{\partial x} - \frac{\partial(uv)}{\partial y} - \frac{\partial \tilde{\phi}}{\partial x} + \left(\frac{1}{Re}\right)\frac{\partial}{\partial y}\left(\frac{\partial u}{\partial y} - \frac{\partial v}{\partial x}\right) + \frac{1}{Fr^2} g_x \right]_{t=t_n}, \tag{4}$$

$$\frac{\partial \tilde{v}}{\partial t} = \left[-\frac{\partial(uv)}{\partial x} - \frac{\partial(v^2)}{\partial y} - \frac{\partial \tilde{\phi}}{\partial y} - \left(\frac{1}{Re}\right)\frac{\partial}{\partial x}\left(\frac{\partial u}{\partial y} - \frac{\partial v}{\partial x}\right) + \frac{1}{Fr^2} g_y \right]_{t=t_n}, \tag{5}$$

using the correct boundary conditions for $\mathbf{u}(\mathbf{x}, t_n)$.

(iii) Solve (a discrete version of) the Poisson equation

$$\nabla^2 \psi(\mathbf{x}, t_{n+1}) = \nabla \cdot \tilde{\mathbf{u}}(\mathbf{x}, t_{n+1}).$$

(iv) Compute the corrected velocity field

$$\mathbf{u}(\mathbf{x}, t_{n+1}) = \tilde{\mathbf{u}}(\mathbf{x}, t_{n+1}) - \nabla \psi(\mathbf{x}, t_{n+1}).$$

(v) Compute the pressure

$$\phi(\mathbf{x}, t_{n+1}) = \tilde{\phi}(\mathbf{x}, t_{n+1}) + \psi(\mathbf{x}, t_{n+1})/\delta t_n.$$

Thus, GENSMAC solves the momentum equations (1) and (2) explicitly and a sparse symmetric system (the discrete Poisson equation) for the correction velocity potential function ψ. The essential point is that at step (ii), the correct vorticity is obtained, but mass is not conserved. Steps (iii) and (iv) supply a corrected velocity field that satisfies the continuity equation. Particles are created at the inlets and are injected into the containment region to represent the fluid. These are virtual particles whose co-ordinates are stored at each time step and then updated by solving

$$\frac{\mathrm{d}x}{\mathrm{d}t} = u, \qquad \frac{\mathrm{d}y}{\mathrm{d}t} = v,$$

by Euler's method. This provides the new co-ordinates of each particle, and hence a snapshot of the fluid at any point in time. These snapshots may then be assembled to form a video sequence.

3. NUMERICAL SIMULATION OF CONTAINER FILLING

The task that confronts us is to effect a comparison between experimentally filling a container with a highly viscous incompressible fluid and its numerical simulation. Buckling of the fluid jet (emanating from the dosing head) is extremely sensitive to both the fluid velocity (more precisely, the Reynolds number—see Tomè and McKee [4]) and the aspect ratio of the container, and consequently is an ideal phenomenon with which to effect a comparison. Thus, the jet buckling phenomenon was studied for two differently shaped containers (see Figure 1).

The following data were employed:

- Square cell
  $L = 50$ mm
  $D = 3, 4, 5$ mm (inlet nozzle size)

Dynamic viscosity (μ) = 1, 5, 10 Pa
Density (ρ) = 1000 kg m^{-3}
Entry speed at nozzle (U) = 0.5, 1.0. 5.0, 10.0 m s^{-1}
– The no-slip condition was applied at the walls.

- Trapezoidal cell
  $L1 = 60$ mm
  $L2 = 85$ mm
  $L3 = 70$ mm
  $D = 15$ mm (inlet nozzle size)
  Dynamic viscosity (μ) = 1, 5, 10, 20, 50 Pa s
  Density (ρ) = 1000 kg m^{-3}
  Entry speed at nozzle (U) = 0.5, 1.0, 5.0, 10.0, 20.0 m s^{-1}
  – The no-slip condition was applied at the walls.

The code was run with all combinations of the data above and several different flow patterns were observed. In total, 36 runs for the square container and 25 runs for the trapezoidal container were performed. A mesh size of 100×100 cells ($\delta x = \delta y = 0.5$ mm) was used for the square container and a mesh size of 85×60 cells ($\delta x = \delta y = 1$ mm) for the trapezoidal container. The non-dimensional time step size was restricted according to

$$\delta t < \frac{\delta x^2}{8} \text{ if } Re > 1 \quad \text{or} \quad \delta t < \frac{\delta x^2}{8} Re \text{ if } Re \leq 1.$$

A convergence criterion for the conjugate gradient (CG) method was chosen to be $\epsilon = 10^{-5}$ for all runs. The CG solver converged for all data, verifying its robustness as implemented in GENSMAC. The parameters governing each problem were defined by

$$Re = \frac{UD}{v} \quad \text{and} \quad \frac{1}{Fr^2} = \frac{gD}{U^2},$$

were D denotes the nozzle slit width and U the nozzle inlet velocity. For the above data it is easily verified that the Reynolds number lies in the range [0.15, 50] for the square container and in the range [0.15, 300] for the trapezoidal container. A variety of flow patterns were obtained, some of which are now presented. Details of all runs performed can be found in Tomé *et al.* [5].

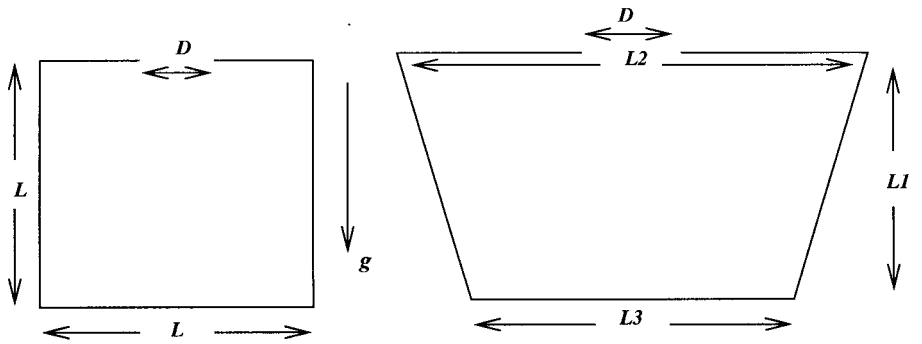

Figure 1. Square and trapezoidal containers used in the simulations.

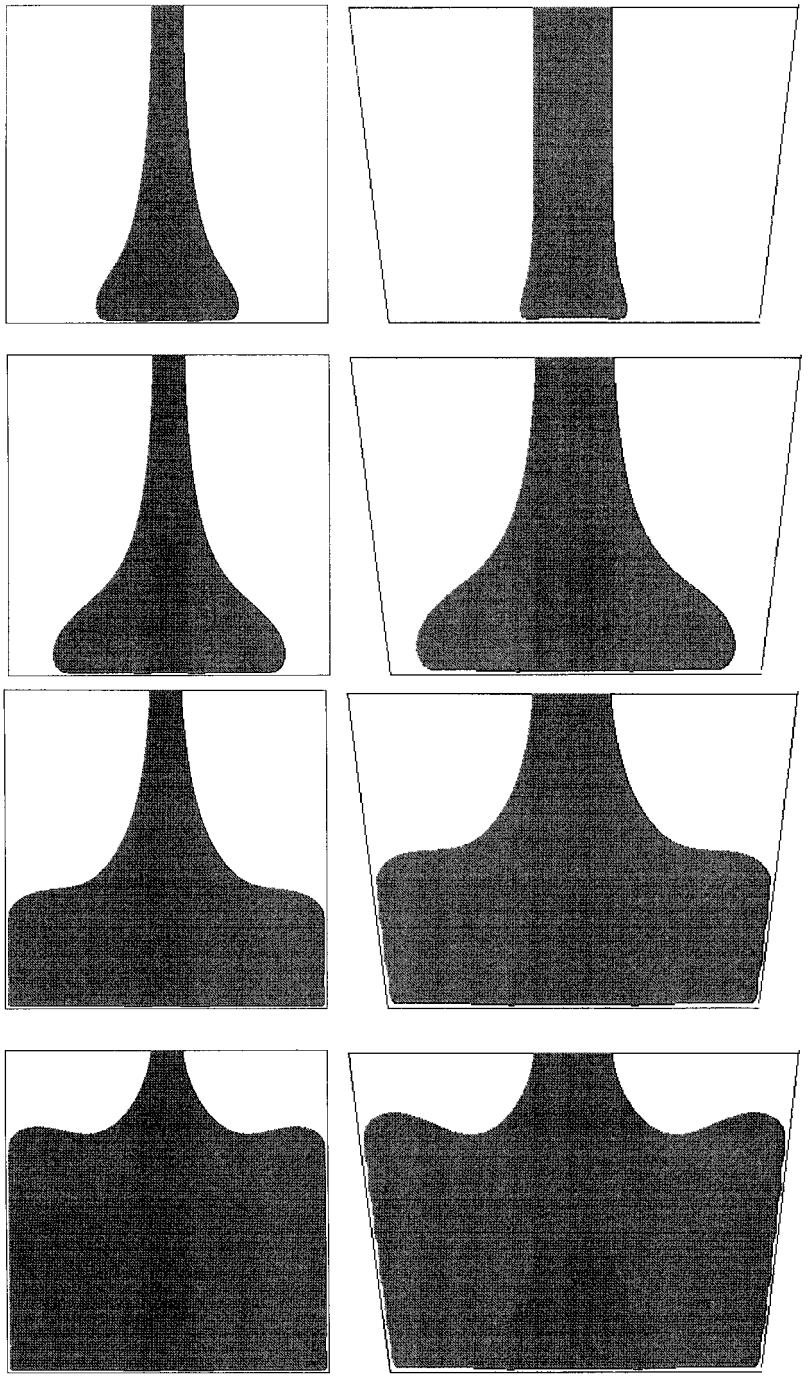

Figure 2. *Steady filling*. Input data employed: $U = 1.0$ m s^{-1}, $D = 5$ mm and $v = 0.005$ m^2 s^{-1} ($Re = 1$, square container); $U = 1.0$ m s^{-1}, $D = 15$ mm and $v = 0.010$ m^2 s^{-1} ($Re = 1.5$, trapezoidal container).

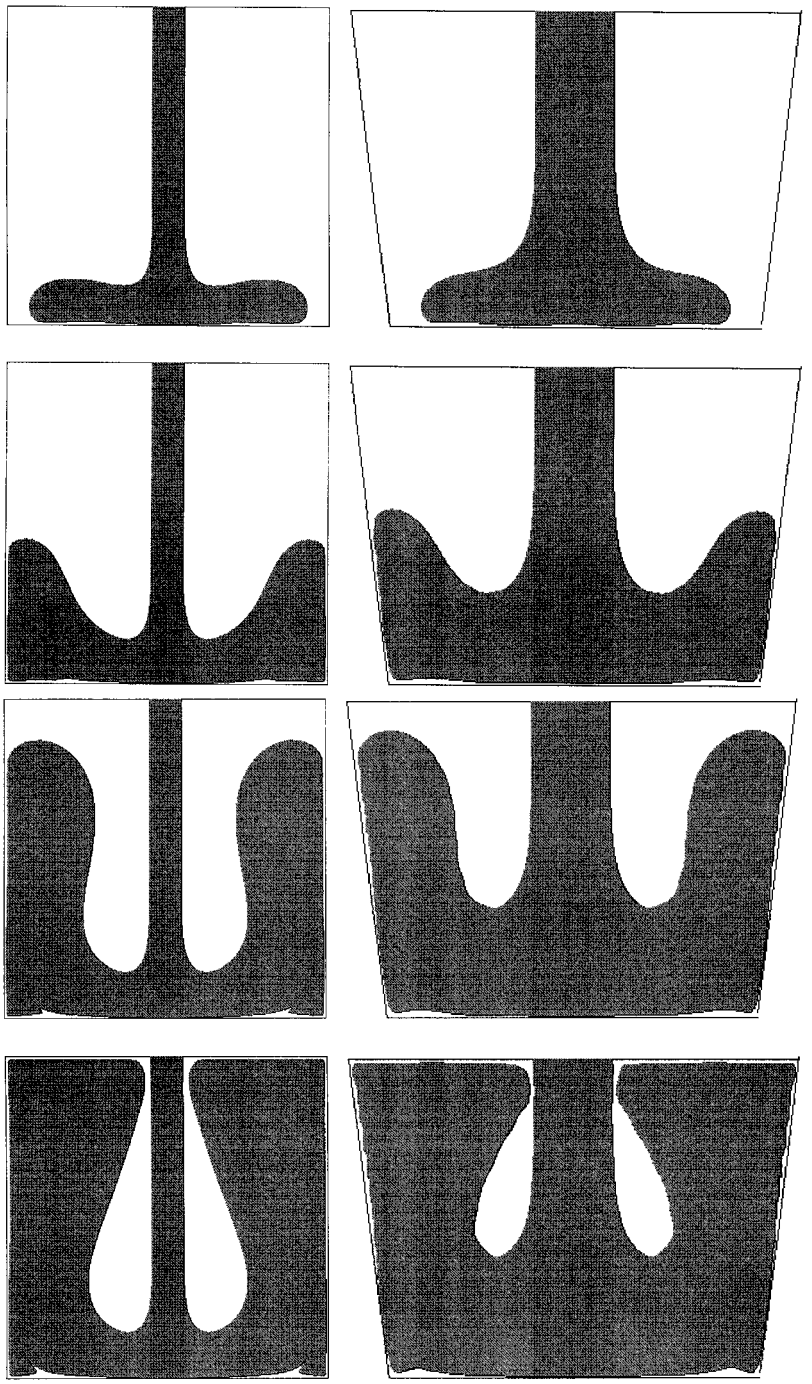

Figure 3. *Splashing*. Input data employed: $U = 5$ m s^{-1}, $D = 5$ mm and $v = 0.001$ m^2 s^{-1} ($Re = 25$, square container); $U = 5.0$ m s^{-1}, $D = 15$ mm and $v = 0.005$ m^2 s^{-1} ($Re = 15$, trapezoidal container).

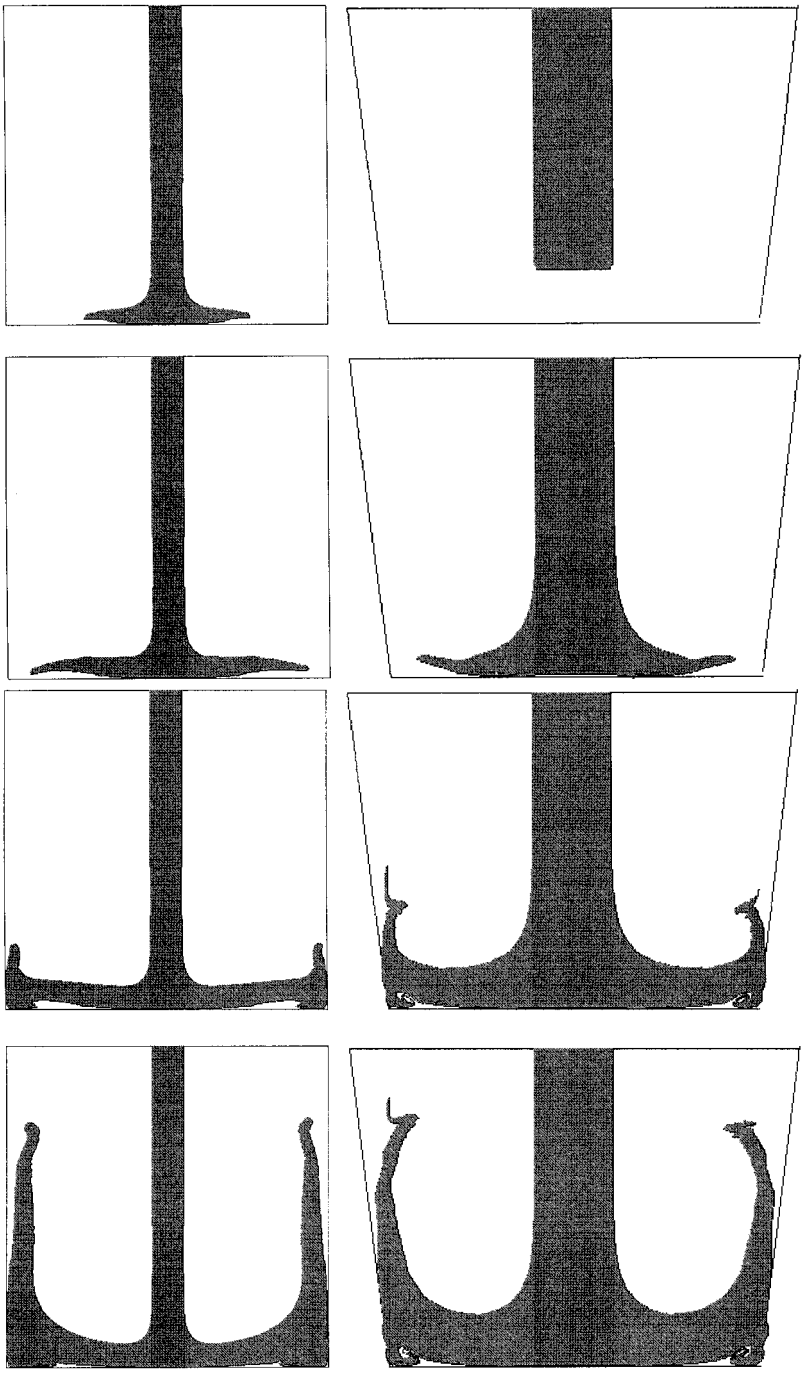

Figure 4. *Spluttering*. Input data employed: $U = 10.0$ m s^{-1}, $D = 5$ mm and $v = 0.001$ m^2 s^{-1} ($Re = 50$, square container); $U = 10.0$ m s^{-1}, $D = 15$ mm and $v = 0.001$ m^2 s^{-1} ($Re = 150$, trapezoidal container).

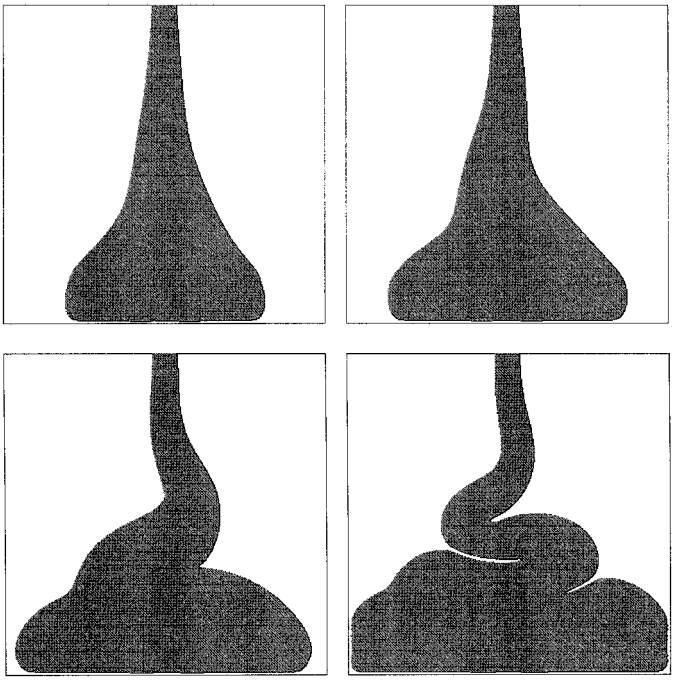

Figure 5. *Buckling jet*. Input data employed: $U = 0.5$ m s^{-1}, $D = 4$ mm and $\nu = 0.010$ m^2 s^{-1} ($Re = 0.2$).

(a) *Steady filling:* Jet fills the container gradually. Figure 2 displays several snapshots of this flow pattern for both containers.
(b) *Splashing:* The jet breaks up and splashes back causing secondary jet flows that rejoin the main jet forming internal bubbles. Figure 3 displays several snapshots of two runs showing this feature.
(c) *Spluttering:* Jet reaches the bottom of the container and splashes back separating from the container bottom. It then strikes the side walls forming secondary jets that also separate from the side walls. Figure 4 presents several snapshots of two runs displaying spluttering.
(d) *Impinging jet buckles:* Jet reaches the bottom of the container and becomes unstable. After a short time the jet becomes asymmetrical and starts to buckle. This phenomenon was observed only for the square container. Figure 5 displays several snapshots of a run in which buckling occurred.
(e) *Jet thinning:* For small inlet velocities, the jet narrows due to gravity forces (small Froude number). This pattern has been observed for both types of containers. Figure 6 provides a single snapshot of two runs displaying jet thinning.

4. MODEL NEWTONIAN FLUIDS

Numerical simulations were performed for a range of viscosities from 1 to 50 Pa. For the experimental work it was decided to use glucose syrup solution to cover this range, since it could be easily prepared in the quantities required for the experiments and the experimental rig could be easily cleaned after each experiment. It is difficult to find truly Newtonian fluids in this viscosity range and the glucose syrup solutions did display some shear thinning behaviour.

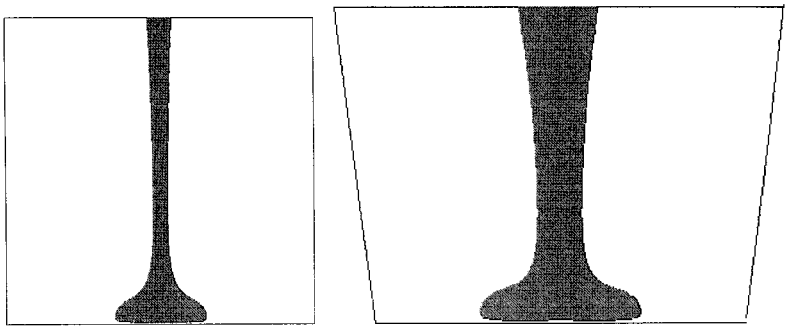

Figure 6. *Jet thinning*. Input data employed: $U = 0.5$ m s^{-1}, $D = 4$ mm and $v = 0.001$ m^2 s^{-1} ($Re = 2$, square container); $U = 0.5$ m s^{-1}, $D = 15$ mm and $v = 0.001$ m^2 s^{-1} ($Re = 7.5$, trapezoidal container).

However, this was fairly small, with only a decrease in the viscosity of approximately 10% over a shear rate range of 1–500 s^{-1}, and an average value was chosen. Some preliminary experiments were carried out to determine the concentrations of glucose syrup required to give the desired viscosities. The glucose syrup used was Cerestar MS (Cerestar UK Ltd) and the viscosity measurements were made on a Haake VT500 viscometer using SV2 coaxial cylindrical geometry. The effect of temperature and concentration on viscosity were measured and are displayed in Figure 7. Figure 8 shows that temperature dependence fits an Arrhenius relationship. Finally, the densities of a number of concentrations were also measured and these were plotted in Figure 9. In the numerical simulations the density of water was used. Since the measured densities were greater than unity it is clearly not possible to match them. To resolve this problem it is useful to consider what are the important hydrodynamics parameters that govern the flow behaviour during filling. The most crucial non-dimensional parameter is the Reynolds number

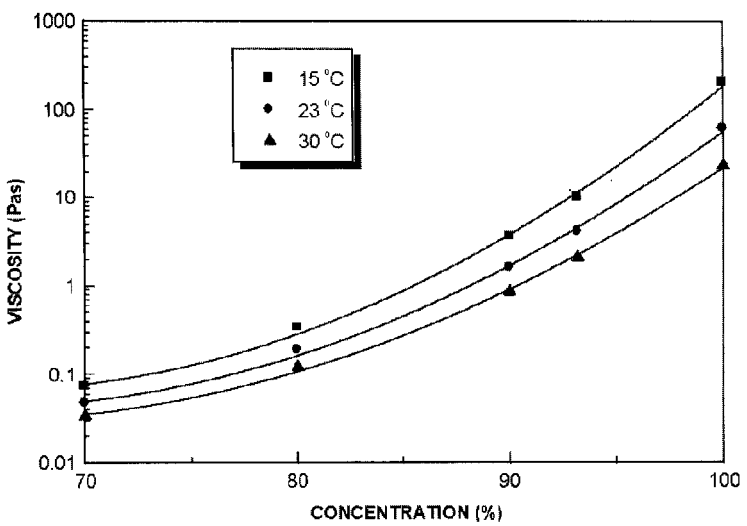

Figure 7. Effect of concentration and temperature on viscosity of glucose syrup solutions.

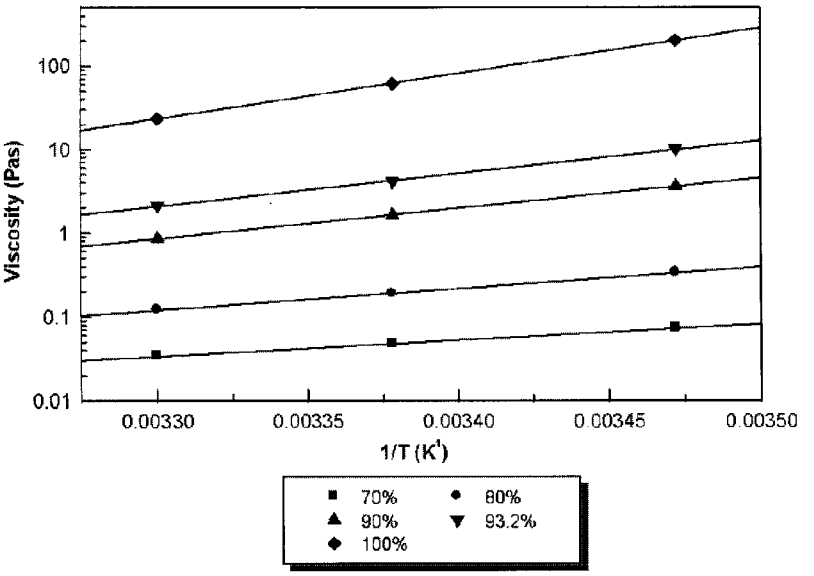

Figure 8. Temperature dependence of viscosity of glucose syrup for different concentrations.

$$Re = \frac{UD}{v} = \frac{\rho UD}{\mu},$$

where D, U, μ, v $(=\mu/\rho)$ and ρ are defined in Section 2.

Therefore, although it was not possible to match both the dynamic viscosity and the density, it was possible to match the kinematic viscosity, and hence the Reynolds number. In practice, this meant that the dynamic viscosities of the glucose syrup solution used were higher than those used in the simulations by a factor equal to the ratio of the densities of the solutions to that of water.

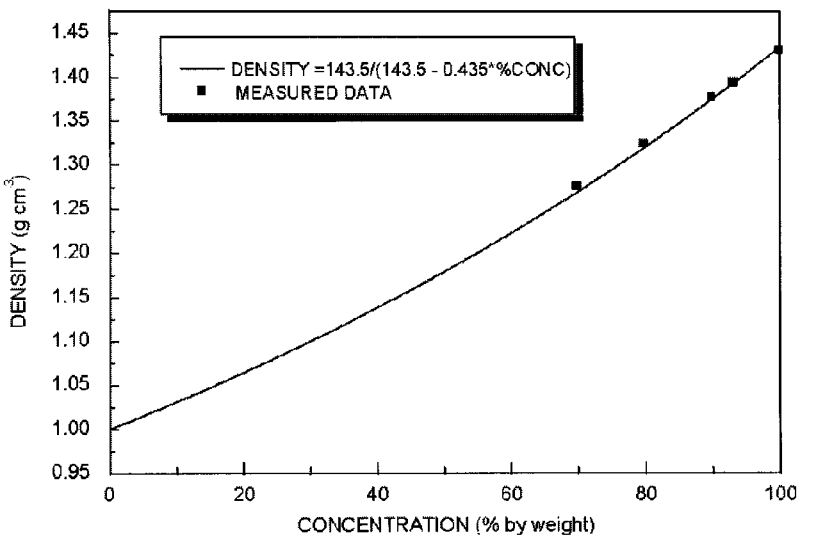

Figure 9. Effect of concentration on density of glucose syrup solutions.

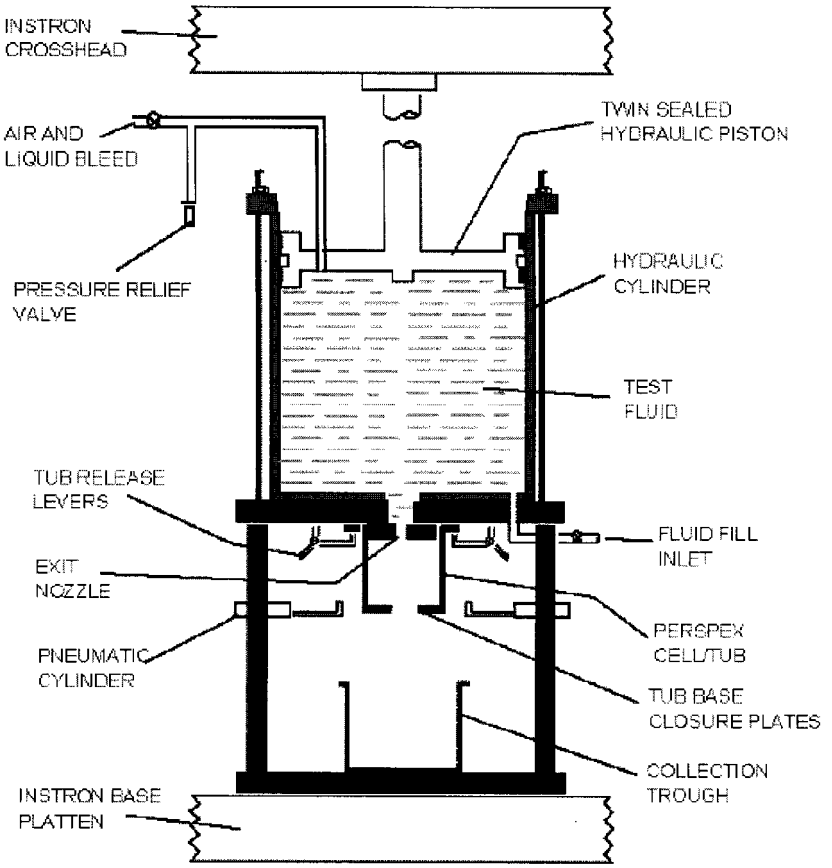

Figure 10. Instron 4204 employed in the experiments.

5. THE EXPERIMENTAL SYSTEM

It was important to design an experimental system capable of providing jet velocities at the nozzle as large as possible in order to be able to make an extensive comparison with the code; and for this reason it was decided to build a rig based upon the Instron Model 4204. A schematic diagram of the experimental rig is shown in Figure 10. It consists of a 250 mm diameter cylinder and piston assembly capable of forcing fluid through the required size of nozzle at a constant speed. Two white light sources were placed either side of the cell to provide illumination during the filling process. A Hitachi video camera was used to video the filling. This had a frame rate of 50 s^{-1}, $\times 8$ magnification, and the shutter speed was set to $\frac{1}{1000}$ s with a *Fr* number of 1.2. The camera had a pixel resolution of 470000 pixels. The fluid used in the experiments was coloured using a red dye and videotaped against a white background to make the fluid boundaries clearly visible. The Instron cross-head is only capable of travelling at 1800 mm min^{-1} (0.3 m s^{-1}); the large diameter cylinder was chosen to amplify the jet speeds to the range 0.5–5 m s^{-1}. This range of velocity was found appropriate: in the food industry fluid velocities for filling of margarine tubs are in the range 0.5–1 m s^{-1}, while this can increase to 5–10 m s^{-1} for mould filling.

GENSMAC is a two-dimensional code and clearly truly two-dimensional flow cannot be achieved experimentally. However, by using nozzles that were long relative to their (slit) width allowed reasonable approximation. Figure 11 shows the nozzles that were used. The nozzles were attached to the underside of the cylindrical barrel and positioned such that their long axis was in line with the axis through the lens of the video camera. The nozzles used for filling the square cell were all 50 mm in length, giving a minimum aspect ratio of 10 for the 5 mm nozzle. For the filling of the trapezoidal cell the nozzle was 75 mm long, and since the nozzle width was 15 mm, this gave a aspect ratio of 5. In practise, some asymmetry was observed in the z-direction (i.e. in the direction out of the page in Figures 13–17), particularly for low velocities and high viscosity fluids. For the filling of the square cell this was a small effect that manifested itself as a slight bowing inwards of the jet at either end by approximately 5% of the length. In the case of the filling of the trapezoidal cell, the effect was greater, particularly at low velocities, and the bowing inwards at the ends of the jet could be as high as 10–20% of the length.

Figure 12 displays the containers that were used. They were made of Perspex to allow observation of the filling and have either square or trapezoidal cross-sections, with the release clamps in such a way that the nozzle formed their lids. The top closure plate in the trapezoidal cell is used to seal the nozzle opening and is opened prior to performing a run. For the square cell such a plate was not necessary because the nozzles were much smaller and the fluid was held in place by surface tension.

From the point of view of achieving high jet velocities, clearly the larger the diameter of the cylinder the better. However, this would require increased piston pressure and this had to be contained within the specification of the Instron frame. The final design was a compromise between achieving the desired jet velocities and limiting the force on the Instron frame, and as a consequence it was only possible to obtain jet velocities of 5 m s^{-1} for the square container for the most viscous fluids. However, for the lowest viscosity fluid and the smallest nozzle width—3 mm—a jet velocity of 9.9 m s^{-1} was achievable. This was close to the 10 m s^{-1} used in the simulations. In fact most of the interesting filling behaviour occurs around this velocity, and the only simulated behaviour that could not be observed experimentally was that of splattering, which only occurs at higher jet velocities.

Air entrapment during filling of the cylinder was potentially a problem. To avoid this, the cylinder was filled from the bottom as indicated in Figure 10. The procedure was to place the fluid reservoir on a shelf above and to the side of the Instron. A tap at the base of the reservoir was then connected to the filling port on the rig by a plastic tube, and the cylinder allowed to

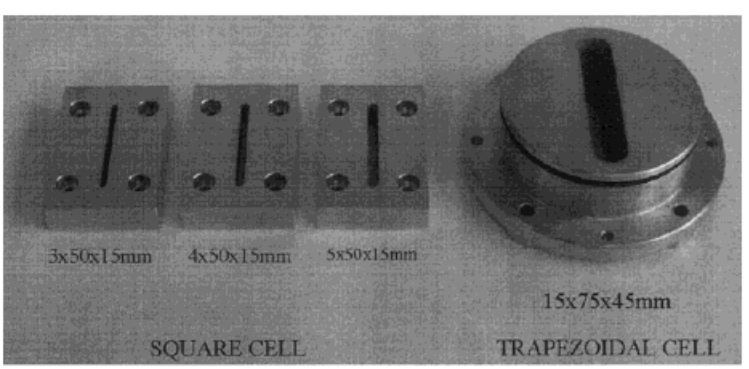

Figure 11. Nozzles employed in the experiments.

fill under gravity and with the piston engaged. When the cylinder was full the fluid passed through an air and liquid bleed in the piston, which could then be closed. The bleed also incorporated a pressure relief valve as a safeguard against the pressure in the cylinder becoming too high.

One assumption of the numerical model was that at time $t = 0$, the fluid is stationary and that at $t > 0$ it was travelling at a constant velocity. In practice, however, there is an initial acceleration of the fluid and this needs to be allowed for in the experiment. This was achieved by having an opening in the base of the container (the Perspex cell/tub in Figure 10), just below the nozzle, through which the fluid jet has to pass. The jet was then allowed to attain its steady velocity before the base of this container was closed using two plates driven by pneumatic cylinders. The two plates met in the centre of the container and care had to be taken to ensure that they closed together; otherwise asymmetric filling could occur.

6. EXPERIMENTAL DIFFICULTIES AND PROCEDURE

Initials trials with the system highlighted a few problems that had to be overcome. Firstly, fluid flow along the length of the container (or collection trough in Figure 10), i.e. in a direction out of the page, distorted the filling pattern. To correct for this, baffle plates were inserted into the

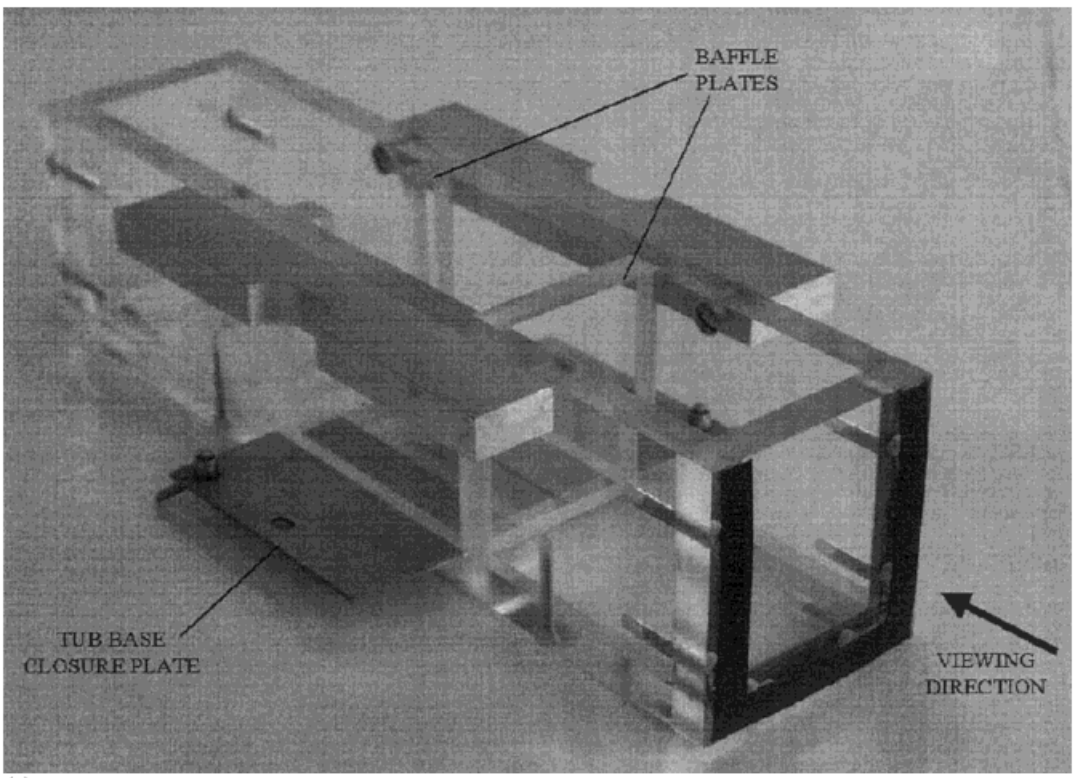

Figure 12. Perspex cells used in the experiments: (a) square cell ($L = 5$ cm, z-direction $= 7.5$ cm), (b) trapezoidal cell ($L_1 = 6$ cm, $L_2 = 8.5$ cm, $L_3 = 7$ cm, z-direction $= 10$ cm). See Figure 1.

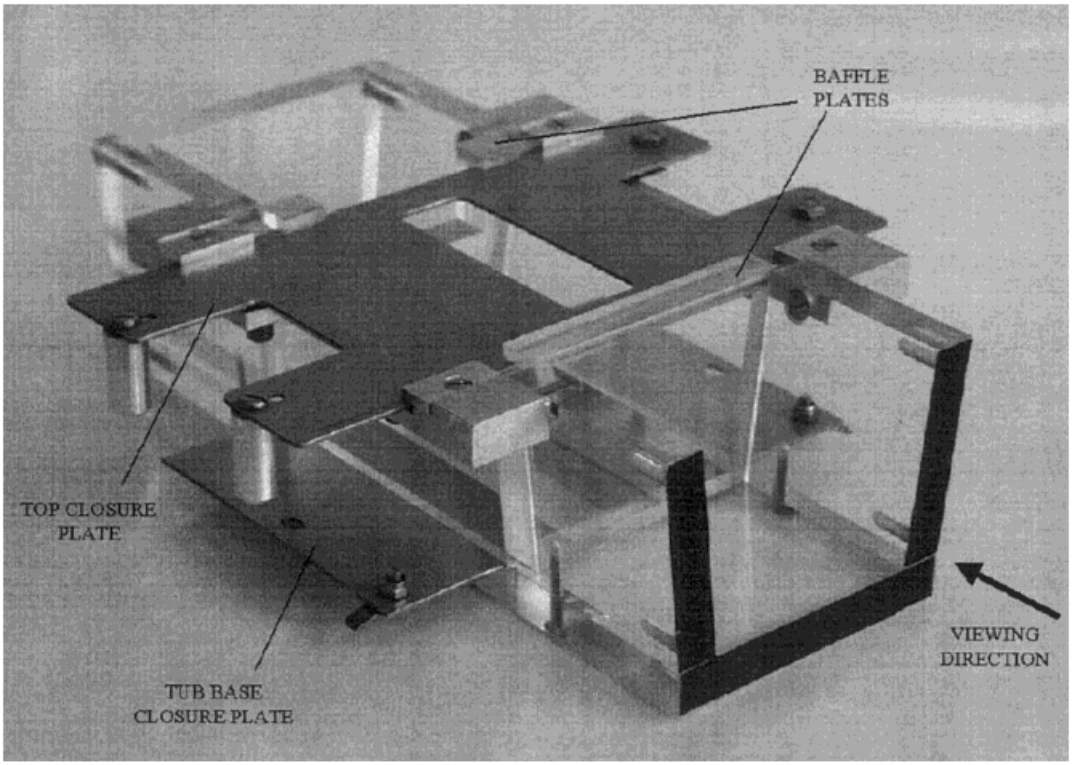

(b)

Figure 12 (*Continued*)

collection trough just beyond the ends of the nozzle in order to limit flow in this direction (see Figure 12). A disadvantage of this arrangement was that fluid could flow up the surfaces of these plates and obscure the flow pattern of the bulk fluid. In most cases this was not a problem, since the layer of fluid on the plates was sufficiently transparent to allow the bulk flow behaviour to be observed. A second problem was caused by electrostatic attraction between the fluid jet and the Perspex cell. This occurred when the flow was initiated prior to closure of the Perspex cell, and resulted in the jet being pulled to one side. This was particularly a problem at low velocities and resulted in the jet fouling on the side of the collection trough. This problem was resolved by treating the surfaces of the Perspex cell with an anti-static fluid (Destatol, Elgar Phosphors Chemicals Ltd.) prior to every run. A third problem was that the jet exiting from the nozzle was frequently not vertical. This led to asymmetry in the observed filling pattern. This was found to be due to very small imperfections on the inside walls of the nozzles (see Figure 11), and required a new set to be cut using a more accurate milling technique.

7. RESULTS AND COMPARISONS

Two shapes of collection troughs were chosen, namely a square container and a wedge shaped container (see Figure 1).

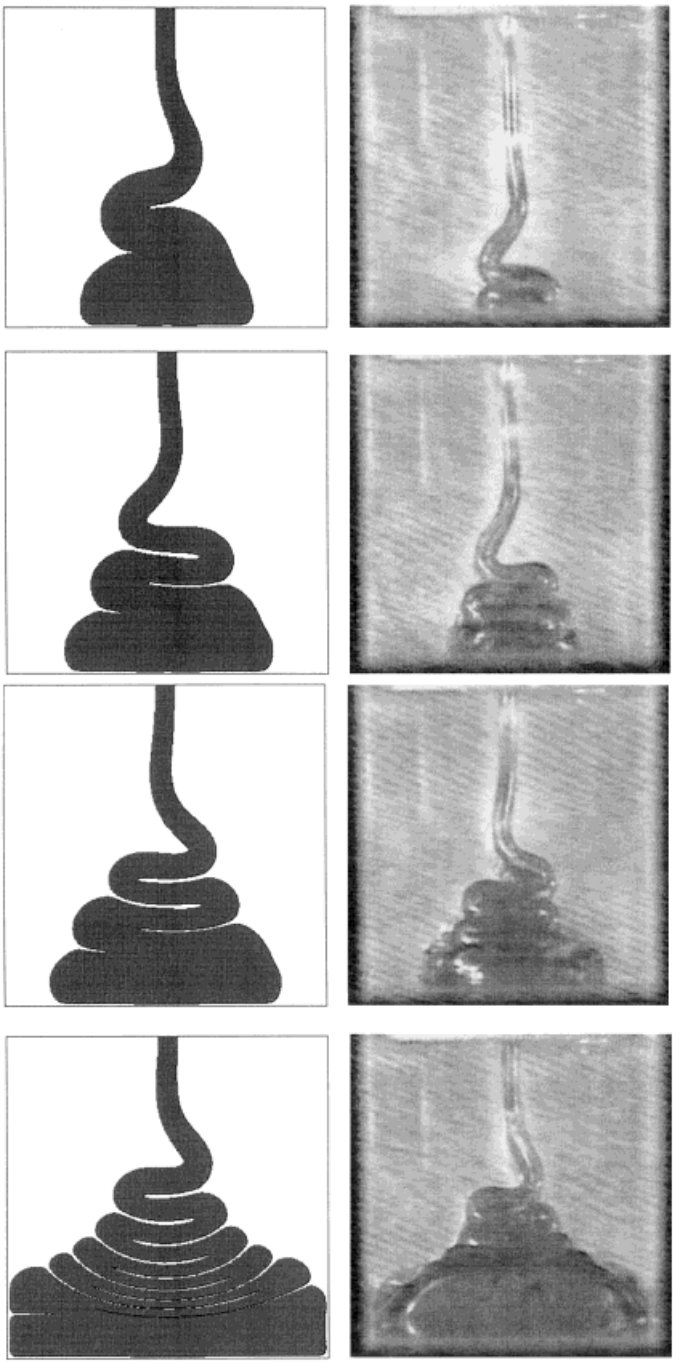

Figure 13. Comparison between numerical (left) and experimental (right) of jet buckling. Input data are: $D = 3$ mm, $U = 0.5\ \mathrm{m\,s^{-1}}$ and $v = 0.010\ \mathrm{m^2\,s^{-1}}$; $Re = 0.15$.

A great many numerical simulations were carried out and a large number of experiments were undertaken. These are more fully reported by Jarvis *et al.* [6]. Here we give comparative results for four Reynolds numbers, $Re = 0.15$, 0.8, 2.5 and 25. These can be seen in Figures 13–16 respectively. Note that the numerically simulated results are on the left.

Figure 13 illustrates planar jet buckling. Note that pronounced buckling occurs much earlier in practice than in the simulated fluid. With the higher Reynolds number of 0.8 (Figure 14) we observe that there is no longer buckling and good agreement exists between the simulated and experimental results. For the manufacturer this is a good fill: there is no buckling while at the same time no splashing or spluttering. As the Reynolds number is increased reasonable agreement is obtained (Figure 15). The jet thinning, observable in the simulated results, is just discernible in the experimental results. In practice, it can be seen that the fluid spreads latterly more rapidly than the simulated results predict. Finally, with a Reynolds number of 25, Figure 16 indicates that, but for the lid, spillage would result. Both the simulated and experimental results agree well, showing at least in two dimensions that there is a possibility of air entrapment.

The trapezoidal tub or collection trough does not present substantial surprises. Again, a great deal of experimentation is detailed in Jarvis *et al.* [6]. A single result with Reynolds number equal to 7.5 (Figure 17) is given. This shows good agreement with both the real and simulated fluid emerging from the jet and beginning to climb the side walls of the tub. Once again both exhibit thinning of the jet, although this would appear to be more pronounced in the simulated results.

8. DISCUSSION

Overall the results compare favourably. The largest discrepancy occurs with jet buckling. There are a number of reasons why this might be. Firstly, the code does not contain surface tension and this clearly will have an effect. However, in most cases this effect is negligible as the other result bears out. One must remember that jet buckling is a physical instability: the jet is as likely to buckle to the right as it is to the left, and any small perturbation can initiate buckling. In the numerical simulation this can only be round-off error, but in the experimental rig there are a number of possibilities. For instance, the Instron assembly may not be perfectly vertical, there may be some residual electrostatic attraction on the side walls of the cell, or the inside nozzle walls may still contain small imperfections. Another factor, which is likely to be a dominant one, is that the two plates that close when the fluid jet reaches a steady velocity may not in fact close at exactly the same time or exactly at the centre of the jet. Thus, it is not at all surprising that jet buckling occurs earlier in the experimental rig than it does numerically.

In Figure 15 we observe that spreading takes place more rapidly than the numerical results suggest. However, there are a number of factors that could have an effect. We recall that the glucose syrup solution is not actually Newtonian and exhibits shear thinning. Further, the experimental system is not truly two-dimensional and the baffles, while preventing an apparent depletion of fluid, provide edge effects possibly giving the impression of the fluid spreading further than it really would in their absence.

As a final point, GENSMAC is capable of exhibiting splattering. This only occurs at high velocities. When a small element of fluid detaches itself from the bulk fluid it is treated (numerically) as a solid element subject to Newtonian mechanics. It will, therefore, continue on its initial trajectory until it reattaches itself with the bulk fluid or is expelled from the container or domain of interest. Unfortunately, the Instron specifications did not permit us to reach sufficiently high velocities and thereby test this interesting case.

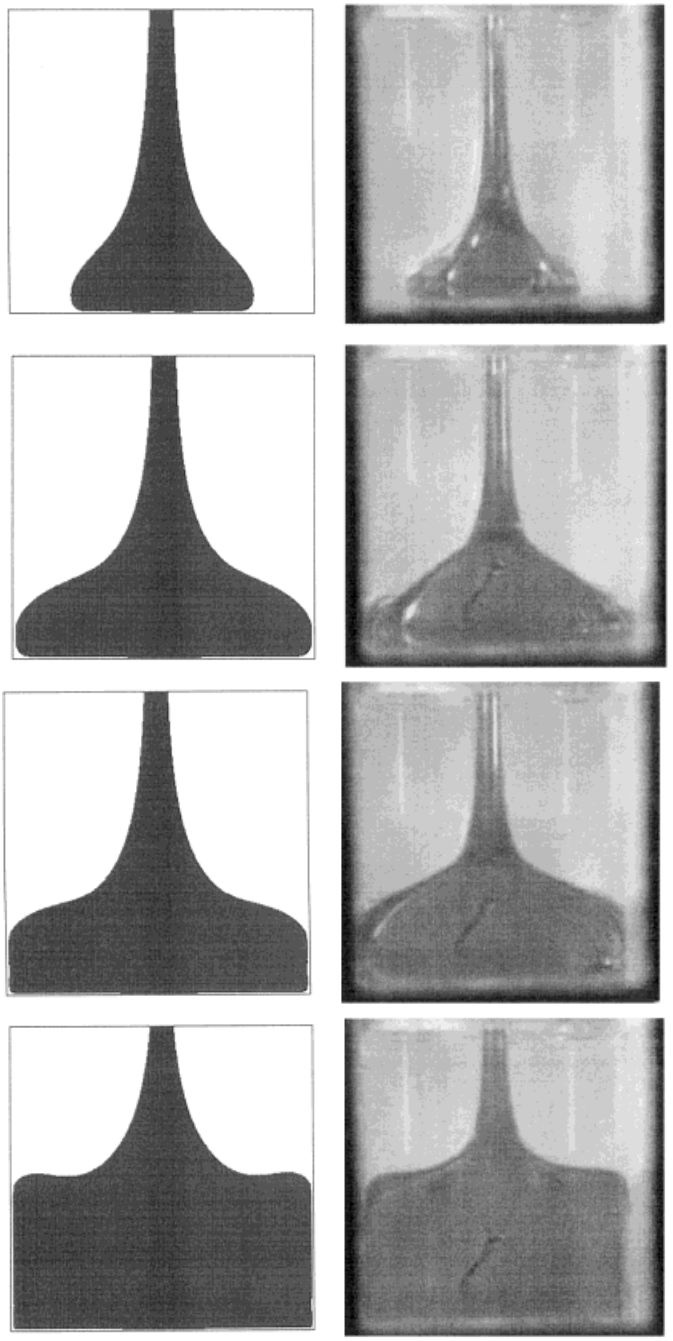

Figure 14. Comparison between numerical (left) and experimental (right). Input data are: $D = 4$ mm, $U = 1.0$ m s^{-1} and $\nu = 0.005$ m^2 s^{-1}; $Re = 0.8$.

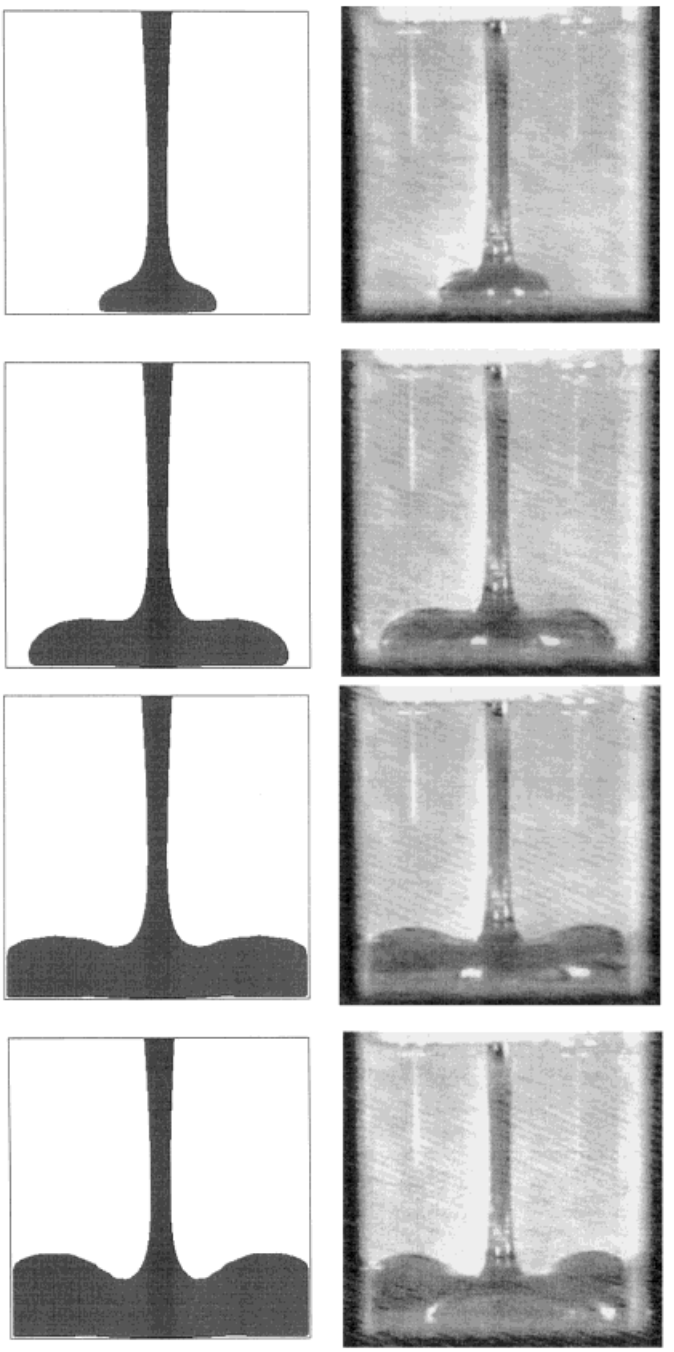

Figure 15. Comparison between numerical (left) and experimental (right). Input data are: $D = 5$ mm, $U = 0.5$ m s^{-1} and $v = 0.001$ m^2 s^{-1}; $Re = 2.5$.

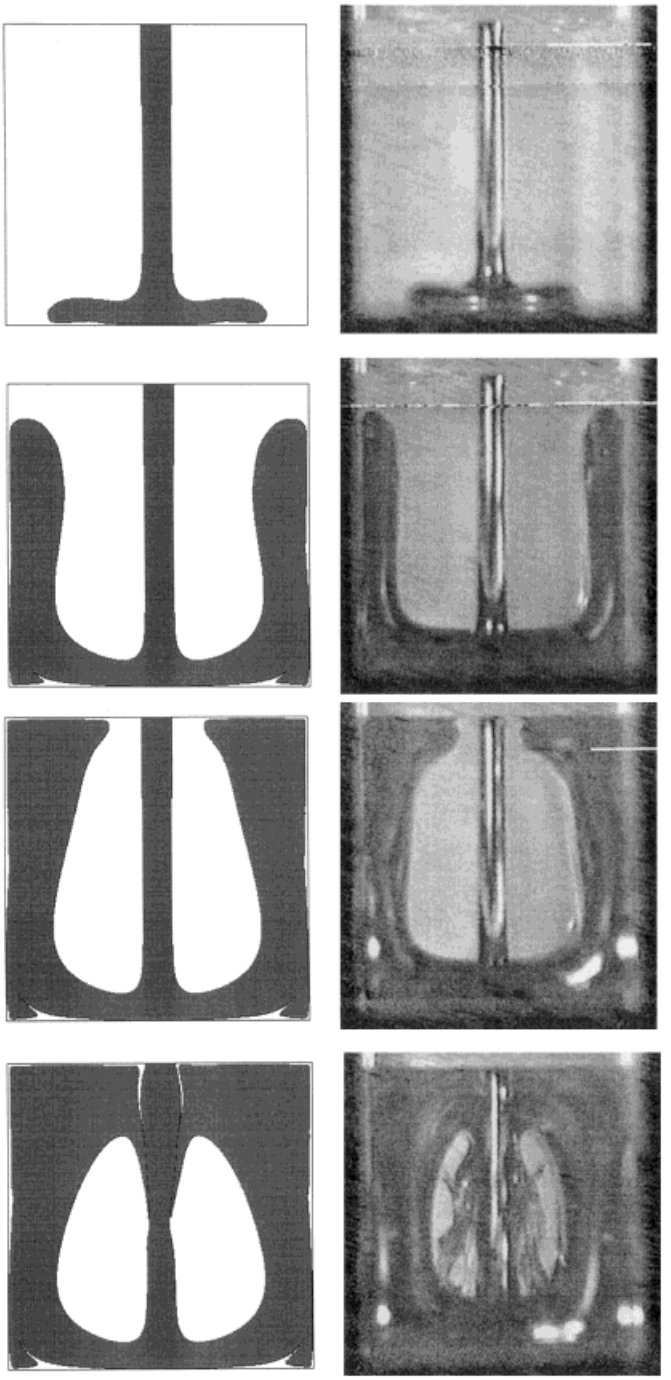

Figure 16. Comparison between numerical (left) and experimental (right). Input data are: $D = 5$ mm, $U = 5.0$ m s^{-1} and $\nu = 0.001$ m^2 s^{-1}; $Re = 25$.

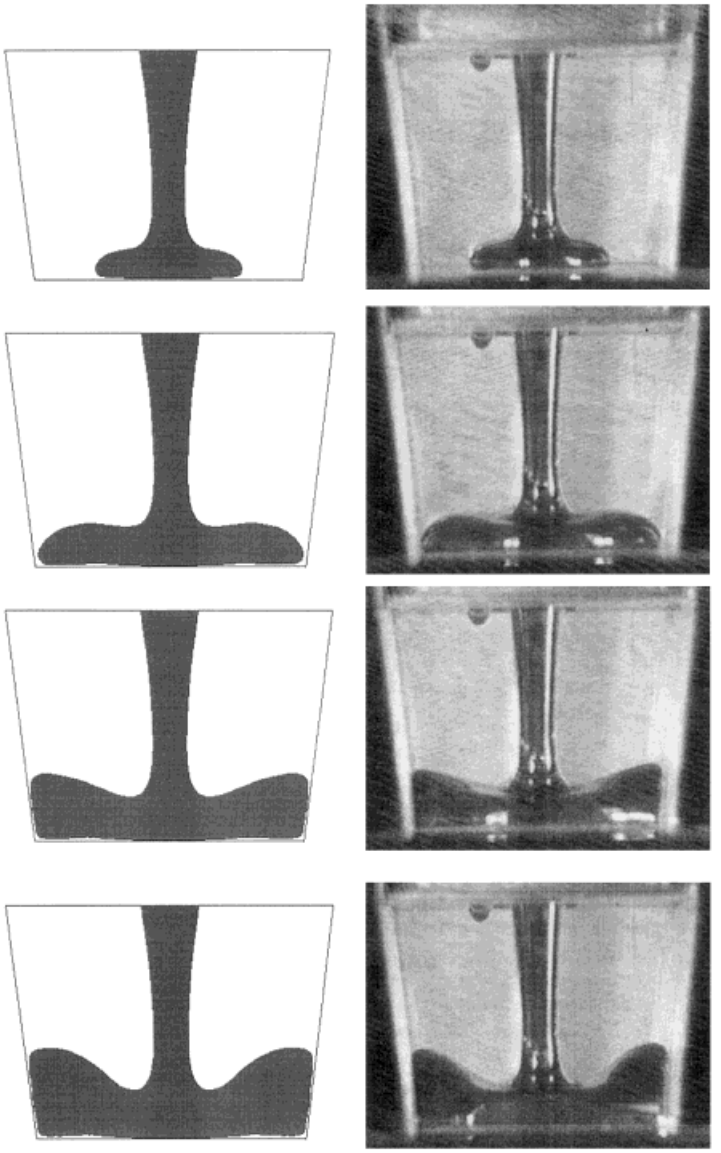

Figure 17. Comparison between numerical (left) and experimental (right). Input data are: $D = 15$ mm, $U = 0.5$ m s^{-1} and $\nu = 0.001$ m^2 s^{-1}; $Re = 7.5$.

ACKNOWLEDGMENTS

This research has been part of project PRAXIS XXI under grant 2/2.1/MAT/380/94. The authors thank the financial support of the Brazilian Agencies FAPESP (Fundação de Amparo a Pesquisa do Estado de São Paulo) and CNPq (Conselho Nacional de Desenvolvimento Científico e Tecnológico).

REFERENCES

1. M.F. Tomé and S. McKee, 'GENSMAC: a computational marker-and-cell method for free surface flows in general domains', *J. Comput. Phys.*, **110**, 171 (1994).
2. F. Harlow and J.E. Welch, 'Numerical calculation of time-dependent viscous incompressible flow of fluid with a free surface', *Phys. Fluids*, **8**, 2182 (1965).
3. M.F. Tomé, B. Duffy and S. McKee, 'A numerical technique for solving unsteady non-Newtonian free surface flows', *J. Non-Newtonian Fluid Mech.*, **62**, 9 (1996).
4. M.F. Tomé and S. McKee, 'Numerical simulation of viscous fluid: buckling of planar jets', *Int. J. Numer. Methods Fluids*, **29**, 705–718 (1999).
5. M.F. Tomé, S. McKee and J. Crilly, 'Numerical simulation of the cavity filling process', *Mathematics Research Report 15*, University of Strathclyde, 1993.
6. D.A. Jarvis, A.J. Patrick, L. Barratt. S. McKee and M.F. Tomé, 'Extensive experimental and numerical investigation of tub filling', *Mathematics Research Report 13*, University of Strathclyde, 1996.

